

Chiral quark models with non-local separable interactions at finite temperature and chemical potential

D. Gómez Dumm^{a †} and Norberto N. Scoccola^{b,c †}

^a *IFLP, Depto. de Física, Universidad Nacional de La Plata,
C.C. 67, (1900) La Plata, Argentina.*

^b *Physics Department, Comisión Nacional de Energía Atómica,
Av.Libertador 8250, (1429) Buenos Aires, Argentina.*

^c *Universidad Favaloro, Solís 453, (1078) Buenos Aires, Argentina.
(July 2001)*

Chiral quark models with non-local covariant separable interactions at finite temperature and chemical potential are investigated. We develop a formalism in which the different quark properties are evaluated taking into account the analytic structure of the quark propagator. In this framework we study the chiral restoration phase transition for several definite non-local regulators, including that arising within the instanton liquid picture. We find that in all cases the chiral transition is of first order for low values of T , turning into a smooth crossover at a certain “end point”. Using model parameters which lead to the physical pion mass and decay constant, we find for the position of this “end point” the values $(T_E, \mu_E) \approx (60 - 70, 180 - 210)$ MeV. We also discuss the special relevance of the first poles of the quark propagator.

12.39.Ki, 11.30.Rd, 11.10.Wx

I. INTRODUCTION

The understanding of the behaviour of strongly interacting matter at finite temperature and/or density is of fundamental interest and has important applications in cosmology, in the astrophysics of neutron stars and in the physics of relativistic heavy ion collisions. From the theory of the quark-gluon interactions, Quantum Chromo Dynamics (QCD), we believe that at zero temperature and density chiral symmetry is spontaneously broken and quarks are confined within hadrons. However, since QCD is asymptotically free, when either the temperature T or the chemical potential μ are high the effective coupling becomes small. Thus, one expects that at a certain point the system undergoes a phase transition (or crossover) to a new phase in which color is screened rather than confined and chiral symmetry is restored. Unfortunately, so far, it has not been possible to obtain detailed information about the corresponding $T - \mu$ phase diagram directly from QCD. In fact, lattice simulations, which work well for zero density and finite temperature, have serious difficulties in dealing with the complex fermion determinant that arises at finite chemical potential [1]. In this situation, different models have been used to study this sort of problems. Among them the Nambu-Jona-Lasinio model [2] is one of the most popular. In this model the quark fields interact via local four point vertices which are subject to chiral symmetry. If such interaction is strong enough chiral symmetry is spontaneously broken and pseudoscalar Goldstone bosons appear. It has been shown by many authors that when the temperature and/or density increase, the chiral symmetry is restored [3]. As an improvement on the local NJL model, some covariant non-local extensions have been studied in the last few years [4]. Nonlocality arises naturally in the context of several of the most successful approaches to low-energy quark dynamics as, for example, the instanton liquid model [5] and the Schwinger-Dyson resummation techniques [6]. It has been also argued that non-local covariant extensions of the NJL model have several advantages over the local scheme. Indeed, non-local interactions regularize the model in such a way that anomalies are preserved [7] and charges properly quantized, the effective interaction is finite to all orders in the loop expansion and therefore there is not need to introduce extra cut-offs, soft regulators such as Gaussian functions lead to small NLO corrections [8], etc. In addition, it has been shown [9] that a proper choice of the non-local regulator and the model parameters can lead to some form of quark confinement, in the sense that the effective quark propagator has no poles at real energies. In a previous letter [10] we have studied the phase diagram of a

[†]Fellow of CONICET, Argentina.

non-local model with a Gaussian regulator. The aim of the present work is to present details of such analysis as well as to extend it to more general cases, such as the Lorentzian regulator and the regulator arising within the instanton liquid model.

This article is organized as follows. In Sec. II we introduce the model and the formalism needed to extend it to finite temperature and density. In Sec. III we discuss how to perform the summation over the Matsubara modes for the expressions obtained previously. Our results for some specific non-local regulators are presented in Sec. IV. Finally, in Sec. V we give our conclusions.

II. FORMULATION

Our starting point is the partition function at zero T and μ ,

$$\mathcal{Z}_0 = \int \mathcal{D}\bar{\psi} \mathcal{D}\psi e^{-S_E}, \quad (1)$$

where S_E stands for the Euclidean action

$$S_E = \int d^4x \left[\bar{\psi}(x) (-i\rlap{\not{D}} + m_c) \psi(x) - \frac{G}{2} j_a(x) j_a(x) \right]. \quad (2)$$

Here m_c is the current quark mass, and the euclidean operator $\rlap{\not{D}}$ is defined as

$$\rlap{\not{D}} = \gamma_4 \frac{\partial}{\partial \tau} + \vec{\gamma} \cdot \vec{\nabla} \quad (3)$$

with $\gamma_4 = i\gamma_0$, $\tau = it$. The current $j_a(x)$ is given by

$$j_a(x) = \int d^4y d^4z r(y-x) r(x-z) \bar{\psi}(y) \Gamma_a \psi(z), \quad (4)$$

where $\Gamma_a = (1, i\gamma_5 \vec{\tau})$ and $r(x-y)$ is a non-local regulator function. The regulator is local in momentum space, namely

$$r(x-z) = \int \frac{d^4p}{(2\pi)^4} e^{-i(x-z)p} r(p). \quad (5)$$

In fact, Lorentz invariance implies that $r(p)$ can only be a function of p^2 , hence we will use for the Fourier transform of the regulator the form $r(p^2)$ from now on.

To proceed it is convenient to deal with bosonic degrees of freedom. Let us perform a standard bosonization of the theory, introducing the sigma and pion meson fields

$$M_a(x) = (\sigma(x), \vec{\pi}(x)). \quad (6)$$

Following the usual steps we obtain a partition function equivalent to that in (1):

$$\mathcal{Z} = \int \mathcal{D}\sigma \mathcal{D}\pi \det A(M_a) \exp \left[-\frac{1}{2G} \int \frac{d^4p}{(2\pi)^4} M_a^2(p) \right], \quad (7)$$

where the operator A in momentum space reads

$$A(M_a) = (-\rlap{\not{p}} + m_c) (2\pi)^4 \delta^{(4)}(p-p') + r(p^2) M_a(p-p') r(p'^2) \Gamma_a. \quad (8)$$

At this stage, we perform the mean field approximation by expanding the meson fields around their translational invariant vacuum expectation values

$$\sigma(x) = \bar{\sigma} + \delta\sigma(x) \quad (9)$$

$$\pi_i(x) = \bar{\pi}_i + \delta\pi_i(x) \quad (10)$$

and neglecting the fluctuations $\delta\sigma(x)$ and $\delta\pi_i(x)$. The mean values of the pion fields vanish due to symmetry reasons. Within this approximation the determinant in (7) is formally given by

$$\det A = \exp \text{Tr} \log A = \exp V^{(4)} \int \frac{d^4 p}{(2\pi)^4} \text{tr} \log [-\not{p} + m_c + \bar{\sigma} r^2(p^2)] , \quad (11)$$

where tr stands for the trace over the Dirac, flavor and color indices, and $V^{(4)}$ is the four-dimensional volume of the functional integral.

Now the corresponding partition function in the grand canonical ensemble for finite temperature T and chemical potential μ can be obtained through the replacement in the integrals in (7) and (11)

$$\int \frac{d^4 p}{(2\pi)^4} F(p_4, \vec{p}) \rightarrow \not{\int}_p F(p_4, \vec{p}) \equiv T \sum_{n=-\infty}^{n=\infty} \int \frac{d^3 p}{(2\pi)^3} F(\omega_n - i\mu, \vec{p}) , \quad (12)$$

where ω_n are the Matsubara frequencies corresponding to fermionic modes, $\omega_n = (2n+1)\pi T$. In performing this replacement we have assumed that the regulator acquires an explicit μ dependence, as it is the case e.g. in the instanton liquid model [11,12]. In the same way we replace the volume $V^{(4)}$ by V/T , V being the three-dimensional volume in coordinate space. The mean field partition function reads then

$$\mathcal{Z}_{MF}(T, \mu) = \exp [-\Gamma_{MF}(T, \mu)] , \quad (13)$$

where the mean field action is given by

$$\frac{T}{V} \Gamma_{MF}(T, \mu) = -4N_c \left(\not{\int}_p \log [p^2 + \Sigma^2(p^2)] \right) + \frac{\bar{\sigma}^2}{2G} \quad (14)$$

with the quark selfenergy $\Sigma(p^2)$ defined as

$$\Sigma(p^2) = m_c + \bar{\sigma} r^2(p^2) . \quad (15)$$

Finally, the grand canonical thermodynamic potential is given by

$$\Omega_{MF}(T, \mu) = -\frac{T}{V} \log \mathcal{Z}_{MF}(T, \mu) = \frac{T}{V} \Gamma_{MF}(T, \mu) . \quad (16)$$

It can be shown that in general this quantity turns out to be divergent. However, it can be regularized by subtracting the corresponding value at zero T and μ , $\Omega_{MF}^{(r)} = \Omega_{MF} - \Omega_{MF}^{(0)}$. Now the minima of the thermodynamic potential are obtained from the solutions of

$$\frac{\partial \Omega_{MF}}{\partial \bar{\sigma}} = 0 \quad (17)$$

which leads to the following gap equation for $\bar{\sigma}$:

$$\bar{\sigma} = 8N_c G \not{\int}_p \frac{\Sigma(p^2) r^2(p^2)}{p^2 + \Sigma^2(p^2)} . \quad (18)$$

Given the thermodynamic potential the expressions for all other relevant quantities can be easily derived. For each flavor the quark vacuum expectation value is given by

$$\langle \bar{q}q \rangle = \frac{\partial \Omega_{MF}}{\partial m_c} = -4N_c \not{\int}_p \frac{\Sigma(p^2)}{p^2 + \Sigma^2(p^2)} , \quad (19)$$

while the quark density turns out to be

$$\rho_q = -\frac{\partial \Omega_{MF}}{\partial \mu} = -4iN_c \not{\int}_p \frac{p_4 + \Sigma(p^2) \partial_{p_4} \Sigma(p^2)}{p^2 + \Sigma^2(p^2)} . \quad (20)$$

In obtaining these last two equations it should be noticed that for each quark flavor only half of the kinetic term in Eq.(14) contributes to the derivatives.

As well known, if the quark selfenergy is momentum independent as in the conventional NJL model, the sums over the Matsubara frequencies indicated in the previous equations can be easily carried out and one obtains rather simple expressions in terms of the usual occupation numbers. This also holds when the selfenergy only depends on the spatial components of the momentum. However, for the covariant regulators we are considering here the situation is more complicated. The main difficulty is that the analytic structure of the quark propagator $S(q) = 1/(-\not{q} + \Sigma(q^2))$ in the complex plane can be much richer in this case: there might be a rather complicate structure of poles and cuts.

In Minkowski space and for $\vec{q} = 0$ the positions of the poles are given by the solutions of

$$q_0^2 - [m_c + \bar{\sigma} r^2(-q_0^2)]^2 = 0. \quad (21)$$

Let us denote the real and imaginary parts of these solutions with r_p and i_p respectively. For nonzero spatial momentum \vec{q} it is easy to see that the poles are located at $z_p = R_p + iI_p$, where

$$R_p = \pm \epsilon_p, \quad I_p = \pm \frac{r_p i_p}{\epsilon_p} \quad (22)$$

with

$$\epsilon_p = \sqrt{\frac{r_p^2 - i_p^2 + \vec{q}^2 + \sqrt{(r_p^2 - i_p^2 + \vec{q}^2)^2 + 4 r_p^2 i_p^2}}{2}}. \quad (23)$$

On the other hand, the possible cuts of the propagator will be given in general by the cuts of the regulator as a function of q . As in the case of the poles, it is convenient to determine first their position in the q_0 plane for $\vec{q} = 0$. Then it is simple to find the position in the general case applying the above equations to all the points along the cuts.

Before going into the explicit evaluation of the Matsubara sums it is useful to analyze the pole and cut configurations in some relevant situations. One important case is that in which the regulator is such that the Minkowski quark propagator has an arbitrary set of poles but no cuts. Within this class of regulators it might exist a situation in which there are no poles along the real axis. As already mentioned, this situation might be interpreted as a realization of confinement [9]. In that case only quartets of poles located at $\alpha_p = r_p \pm i i_p$, $\alpha_p = -r_p \pm i i_p$ appear. On the other hand, if purely real poles do exist they will show up as doublets $\alpha_p = \pm r_p$. It is clear that the number and position of the poles depend on the details of the regulator. For example, if we assume it to be a step function as in the standard NJL model, only two purely real poles at $\pm M$ appear, with M being the dynamical quark mass. For a Gaussian interaction, three different situations might occur. These can be classified according to the value of $\Sigma(0)$ at zero T and μ , which we denote by $\bar{\Sigma}(0)$. For values of $\bar{\Sigma}(0)$ below a certain critical value $\Sigma(0)_{crit}$, two pairs of purely real simple poles and an infinite set of quartets of complex simple poles appear. At $\bar{\Sigma}(0) = \Sigma(0)_{crit}$, the two pairs of purely imaginary simple poles turn into a doublet of double poles with $i_p = 0$, while for $\bar{\Sigma}(0) > \Sigma(0)_{crit}$ only an infinite set of quartets of complex simple poles is obtained. In the case of the Lorentzian interactions, there is also a critical value above which purely real poles at low q_0^2 cease to exist. However, for this family of regulators the total number of poles is always finite. As we see, several physically interesting regulators indeed belong to the “no cuts” group. Unfortunately some other important ones, like that arising within the instanton liquid model, do lead to propagators which present poles and cuts. Thus, it is necessary to consider this more general situation.

III. EVALUATION OF MATSUBARA SUMS

To proceed with the evaluation of the sums over the Matsubara frequencies we assume that the regulator is such that the quark propagator at $\vec{q} = 0$ has the analytic structure shown in Fig. 1a. Whereas the proposed pole distribution is completely general, we consider for simplicity the particular case in which there is a single cut lying along the real axis in the regions $[-\infty, -r_c]$ and $[r_c, \infty]$. Let us consider the sum appearing in the gap equation Eq.(18),

$$S \equiv \int \frac{d^3q}{(2\pi)^3} T \sum_{n=-\infty}^{\infty} F[(\omega_n - i\mu)^2 + \vec{q}^2] = \int \frac{d^3q}{(2\pi)^3} I(\vec{q}^2), \quad (24)$$

where

$$F(q^2) = \frac{\Sigma(q^2)r^2(q^2)}{q^2 + \Sigma^2(q^2)}. \quad (25)$$

In order to evaluate the sum in (24) it is convenient to fix \vec{q} and define $\mathcal{F}(z) \equiv F[(-iz - i\mu)^2 + \vec{q}^2]$, so that the argument of the sum is given by $\mathcal{F}(i\omega_n)$. It is easy to see that the structure of cuts and poles of $\mathcal{F}(z)$ is similar to that shown in Fig. 1a, conveniently translated to the z plane (see Fig. 1b). This translation can be performed by means of Eqs.(22), with an additional shift $R_p \rightarrow R_p - \mu$. We introduce now the auxiliary function

$$f(z) = [1 + \exp(z/T)]^{-1}, \quad (26)$$

which has a set of poles at $z_n = i\omega_n$ with $-T$ as the corresponding residues. Provided that $\mathcal{F}(z)$ has no poles on the imaginary axis, the sum we want to evaluate can be regarded as the sum over the z_n poles of the residues of the function $-\mathcal{F}(z)f(z)$. We can use Cauchy's theorem to get

$$I(\vec{q}^2) = T \sum_{n=-\infty}^{\infty} \mathcal{F}(i\omega_n) = \frac{i}{2\pi} \int_{-i\infty+\delta}^{i\infty+\delta} dz \mathcal{F}(z) f(z) - \frac{i}{2\pi} \int_{-i\infty-\delta}^{i\infty-\delta} dz \mathcal{F}(z) f(z). \quad (27)$$

The integrals in Eq.(27) can be calculated with the help of complex integrals along adequate paths in the z plane. Let us consider the sum

$$\int_{C_1} dz \mathcal{F}(z) f(z) + \int_{C_2} dz \mathcal{F}(z) f(z) + \int_{C_3} dz \mathcal{F}(z) f(z), \quad (28)$$

where the contours C_1 , C_2 and C_3 are shown in Fig. 1b. In the limit $R \rightarrow \infty$, one can make use of Cauchy's theorem to obtain

$$I(\vec{q}^2) = \sum_{R_p > -\mu} \text{Res}[\mathcal{F}(z); z_p] f(z_p) - \frac{1}{\pi} \int_{\sqrt{r^2 + \vec{q}^2 - \mu}}^{\infty} dx \Delta\mathcal{F}(x) f(x) - \frac{i}{2\pi} \int_{-i\infty-\mu}^{i\infty-\mu} dz \mathcal{F}(z) f(z), \quad (29)$$

where $z_p = R_p + iI_p$ are the poles of $\mathcal{F}(z)$, and we have defined

$$\Delta\mathcal{F} \equiv \frac{\mathcal{F}(x + i\epsilon) - \mathcal{F}(x - i\epsilon)}{2i}, \quad (30)$$

which is different from zero along the cut. Notice that for large R the integrals over the round contours are expected to vanish in view of the exponential fall of $f(z)$.

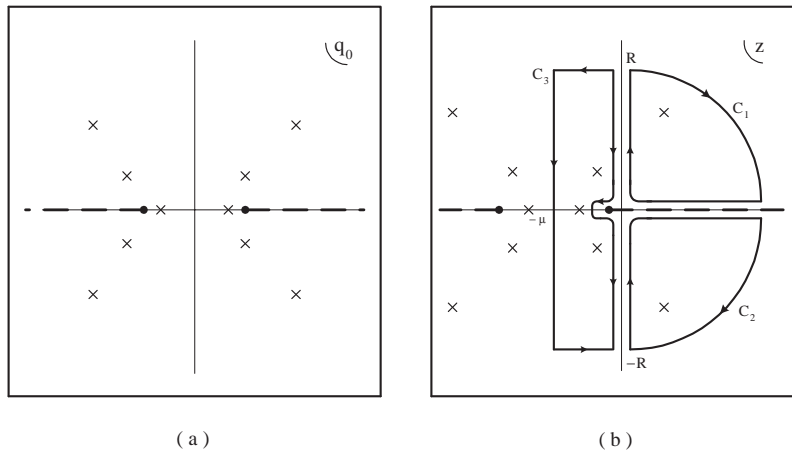


FIG. 1. (a) Poles and cuts of the quark propagator in the q_0 plane for $\vec{q} = 0$. (b) Pole and cut structure of the propagator in the z plane and useful integration paths to evaluate the Matsubara sums.

Now the last integral in the right hand side of (29) can be rewritten by considering the function

$$I_0(\vec{q}^2) = -\frac{i}{2\pi} \int_{-i\infty-\mu}^{i\infty-\mu} dz \mathcal{F}(z) = \frac{1}{2\pi} \int_{-\infty}^{\infty} dq_4 F(q^2), \quad (31)$$

which is nothing but $I(\vec{q}^2)$ in the limit of vanishing T and μ . Notice that

$$-\frac{i}{2\pi} \int_{-i\infty-\mu}^{i\infty-\mu} dz \mathcal{F}(z) f(z) = I_0(\vec{q}^2) + \frac{i}{2\pi} \int_{-i\infty-\mu}^{i\infty-\mu} dz \mathcal{F}(z) f(-z). \quad (32)$$

The last integral in this expression can be evaluated by closing a contour on the left side of the complex plane and using once again Cauchy's theorem. Finally, assuming that the regulator is an analytic function of q^2 , we can use the properties

$$\begin{aligned} \Delta \mathcal{F}(-x - \mu) &= -\Delta \mathcal{F}(x - \mu) = -\text{Im} \mathcal{F}(x - \mu + i\epsilon) \\ \text{Res}[\mathcal{F}(z); z_p] &= -\text{Res}[\mathcal{F}(z); -z_p - 2\mu], \end{aligned} \quad (33)$$

to end up with our main result

$$\begin{aligned} S &= \int \frac{d^4 q}{(2\pi)^4} F(q^2) + 2 \int \frac{d^3 q}{(2\pi)^3} \text{Re} \sum_{\substack{R_p > -\mu \\ I_p \geq 0}} \gamma_p \text{Res}[\mathcal{F}(z); z_p] [n_+(z_p + \mu) + n_-(z_p + \mu)] \\ &\quad - \frac{1}{\pi} \int \frac{d^3 q}{(2\pi)^3} \int_{\sqrt{r_c^2 + \vec{q}^2}}^{\infty} dx \text{Im} \mathcal{F}(x - \mu + i\epsilon) [n_+(x) + n_-(x)], \end{aligned} \quad (34)$$

where the first term corresponds to the value of S at zero temperature and zero chemical potential. The coefficient γ_p is defined as $\gamma_p = 1/2$ for $I_p = 0$ and $\gamma_p = 1$ otherwise, and $n_{\pm}(z)$ stand for the occupation number functions

$$n_{\pm}(z) = f(z \mp \mu) = \frac{1}{1 + \exp[(z \mp \mu)/T]}. \quad (35)$$

It is clear that the steps leading to Eq.(34) can be also followed to evaluate the sums appearing in e.g. the quark vacuum expectation value and the quark density, Eqs.(19) and (20) respectively, once the function $F(q^2)$ is properly redefined. In the case of the regularized thermodynamic potential $\Omega_{MF}^{(r)}$ the situation is somewhat more complicated, since the argument of the sum includes a logarithm that introduces cuts in the z plane outside the real axis. Nevertheless a similar relation can be derived to calculate the corresponding Matsubara sum.

From Eq.(34), it is now easy to obtain the well-known results for the standard NJL model with a three-momentum cut-off Λ [3]. In fact, at the level of mean field approximation such model can be viewed as a particular case of the non-local schemes analyzed above, where the regulator is taken as a theta function in three-momentum space, $r(q^2) = \theta(\vec{q}^2 - \Lambda^2)$ (*i.e.* it is not covariant). Notice that for this regulator there is only one pole at $z_0 = \sqrt{\vec{q}^2 + M^2} - \mu$, $M = m_c + \bar{\sigma}$, with $\text{Res}[\mathcal{F}(z); z_0] = -M/2(z_0 + \mu)$. From the relation $S = \bar{\sigma}/(8GN_c)$ (see Eqs.(24) and (18)) one immediately arrives at the standard NJL gap equation

$$M = m_c + \frac{2GN_c}{\pi^2} \int_0^{\Lambda} dp p^2 \frac{M}{E_p} [1 - n_+(E_p) - n_-(E_p)], \quad (36)$$

where $E_p = \sqrt{p^2 + M^2}$.

IV. RESULTS FOR DEFINITE NON-LOCAL REGULATORS

Having introduced the formalism needed to deal with models with non-local separable interactions at finite temperature and chemical potential, we turn now to show the results of numerical calculations carried out for some particular regulators. We concentrate here in three cases: the Gaussian regulator, the Lorentzian regulator and the regulator arising within the instanton liquid model.

A. Gaussian regulator

Let us analyze a regulator function of the form

$$r(q^2) = \exp(-q^2/2\Lambda^2), \quad (37)$$

where Λ is a parameter of the model, besides the coupling constant G and the current quark mass m_c . We consider here two sets of values for the parameters. Set I corresponds to $G = 50 \text{ GeV}^{-2}$, $m_c = 10.5 \text{ MeV}$ and $\Lambda = 627 \text{ MeV}$, while for Set II the respective values are $G = 30 \text{ GeV}^{-2}$, $m_c = 7.7 \text{ MeV}$ and $\Lambda = 760 \text{ MeV}$. Both sets of parameters lead to the physical values of the pion mass and decay constant. At zero temperature and chemical potential, the calculated values of the chiral quark condensate are $-(200 \text{ MeV})^3$ for Set I and $-(220 \text{ MeV})^3$ for Set II. These values are similar in size to those determined from lattice gauge theory or QCD sum rules. The corresponding results for the selfenergy at $T = \mu = 0$ and zero momentum are $\bar{\Sigma}(0) = 350 \text{ MeV}$ for Set I and $\bar{\Sigma}(0) = 300 \text{ MeV}$ for Set II.

As stated in Sect. II, in the case of a Gaussian regulator the quark propagator has no purely real poles if $\bar{\Sigma}(0)$ is above a critical value $\Sigma(0)_{crit}$, whereas for $\bar{\Sigma}(0) < \Sigma(0)_{crit}$ two pairs of real poles exist. From the explicit expression for the critical selfenergy,

$$\Sigma(0)_{crit} = m_c + \frac{1}{2} \left(\sqrt{m_c^2 + 2\Lambda^2} - m_c \right) \exp \left[- \left(\sqrt{m_c^2 + 2\Lambda^2} + m_c \right)^2 / 4\Lambda^2 \right], \quad (38)$$

it can be easily checked that Set I and Set II correspond to the first and second situations, respectively. Thus, following Ref. [9], Set I might be interpreted as a confining one, since quarks cannot materialize on-shell in Minkowski space.

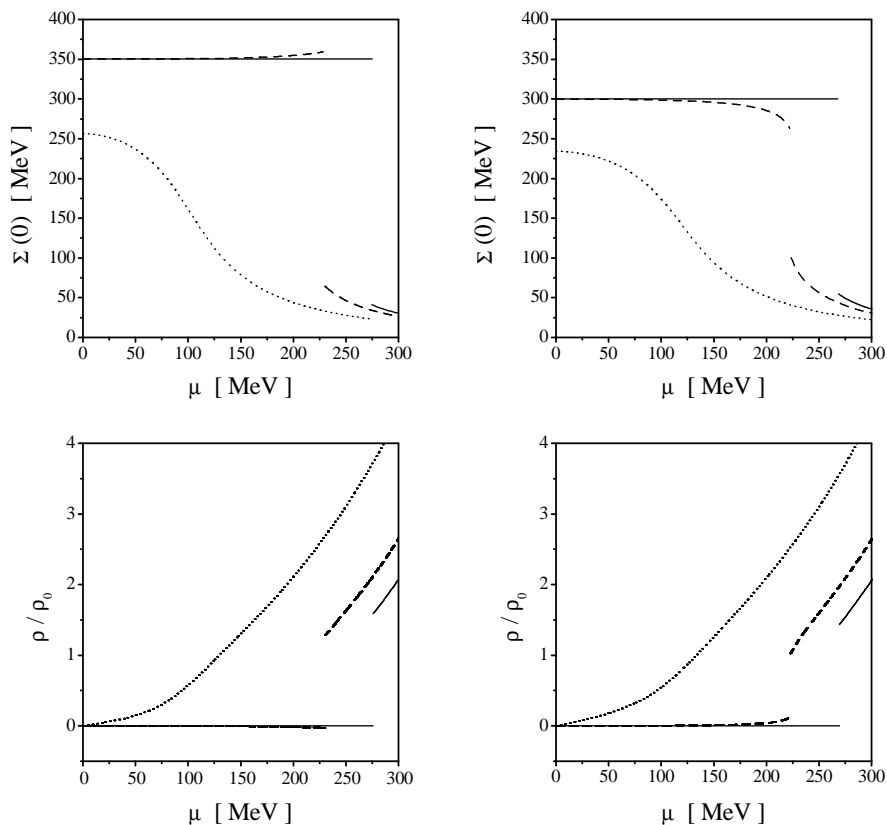


FIG. 2. Behaviour of the selfenergy (upper graphs) and the density (lower graphs) with the chemical potential for three representative values of the temperature. Full lines corresponds to $T = 0$, dashed lines to $T = 50 \text{ MeV}$ and dotted lines to $T = 100 \text{ MeV}$. The left panels display the results for Set I and the right panels those for Set II.

The behaviour of the zero-momentum selfenergy $\Sigma(0)$ as a function of the temperature and chemical potential can be obtained by solving the gap equation for finite T and μ , Eq.(18), where the Matsubara

sum can be evaluated using Eq.(34). In this case the regulator has no cuts in the complex plane, hence the last term of (34) vanishes. A similar procedure can be followed to obtain the quark density ρ for finite T and μ from Eq.(20). Our numerical results are shown in Fig. 2, where we plot $\Sigma(0)$ vs. μ and ρ vs. μ for some fixed values of the temperature. The values of ρ are given with respect to nuclear matter density, $\rho_0 \simeq 1.3 \times 10^6 \text{ MeV}^3$. The left and right panels in the figure correspond to the results for Set I and Set II, respectively. For both sets of parameters we observe the existence of some kind of phase transition at (or around) a given value of the chemical potential which depends on the temperature. The only qualitative differences appear in the behaviour of $\Sigma(0)$ and ρ as functions of μ for low temperatures. For example, for $T = 50 \text{ MeV}$ we observe that in the case of the confining set (Set I) the selfenergy rises with μ (for μ below the critical chemical potential) while the opposite occurs in the case of Set II. As one increases the temperature the behaviour of Set I turns into that of Set II and, eventually, in both cases we obtain a continuous and always decreasing curve. An equivalent behaviour is observed in the case of the density. To obtain our results, we have included in the sums over the poles of the quark propagator only the first few poles close to the origin in the q_0 plane. We have checked, however, that for the range of values of T and μ covered in our calculations, the convergence is so fast that already the first pole gives almost 100% of the full result. Thus, the behaviour of the relevant physical quantities up to (and somewhat above) the phase transition is basically dominated by the first set of poles (doublet or quartets) of the propagator.

We observe that at $T = 0$ there is a first order phase transition for both the confining and the non-confining sets of parameters. As the temperature increases, the value of the chemical potential at which the transition shows up decreases. Finally, above a certain value of the temperature the first order phase transition does not longer exist and, instead, there is a smooth crossover. This phenomenon is clearly shown in the left panel of Fig. 3, where we display the critical temperature at which the phase transition occurs as a function of the chemical potential. The point at which the first order phase transition ceases to exist is usually called “end point”.

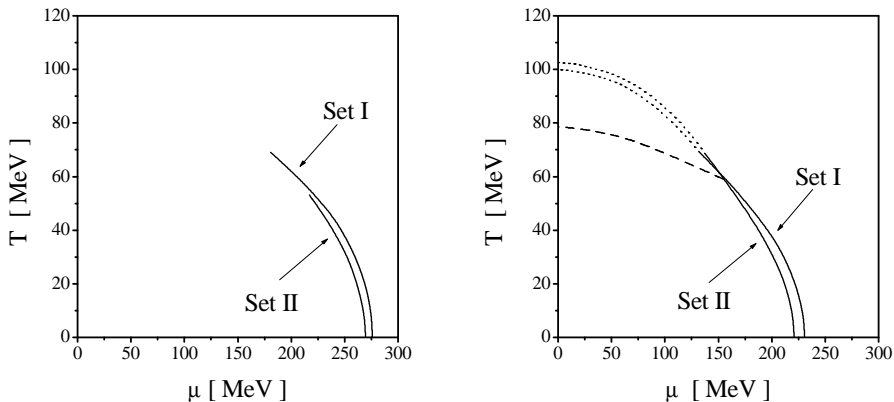


FIG. 3. Critical temperatures as a function of the chemical potential. The left panel corresponds to the case of finite quark masses and the right panel to the chiral limit. In the right panel, the dotted lines correspond to the region of the second order phase transition, while the full lines in both panels indicate the region where a first order transition occurs. The dashed line in the right panel indicates the critical line for deconfinement corresponding to Set I. For chemical potentials somewhat larger than μ_P this line coincides with that of the chiral restoration.

In the chiral limit, the “end point” is expected to turn into a so-called “tricritical point”, where the second order phase transition expected to happen in QCD with two massless quarks becomes a first order one. Indeed, this is what happens within the present model for $m_c = 0$, as it is shown in the right panel of Fig. 3. Some predictions about both the position of the “tricritical point” and its possible experimental signatures exist in the literature [13,14]. In our case this point is located at $(T_P, \mu_P) = (70 \text{ MeV}, 130 \text{ MeV})$ for Set I and $(70 \text{ MeV}, 140 \text{ MeV})$ for Set II, while the “end points” are placed at $(T_E, \mu_E) = (70 \text{ MeV}, 180 \text{ MeV})$ and $(55 \text{ MeV}, 210 \text{ MeV})$, respectively.

In general, for temperatures below the end point there is a range of values of μ where one finds two solutions of the gap equation, *i.e.* there are two values of the selfenergy where the thermodynamic potential shows a local minimum. The situation is illustrated in Fig. 4, where we plot the (renormalized) thermodynamic potential vs. the selfenergy for different values of the temperature and some fixed values of the chemical potential around the phase transition point. The curves in the figure correspond to the parameters of Set II.

In the left panel we consider the case of $T = 0$, where the phase transition occurs at $\mu_c \simeq 270$ MeV, and we plot the values of $\Omega^{(r)}$ for values of μ which are 10 MeV above and below μ_c . The equilibrium point is clearly that corresponding to the absolute minimum in each case. In the central panel we take $T = 50$ MeV, close to the end point temperature of ~ 55 MeV, hence the two minima approach each other and the thermodynamic potential between them is approximately constant. For the right panel the temperature is 100 MeV, well above the end point, therefore one finds only one minimum and the phase transition proceeds through a smooth crossover.

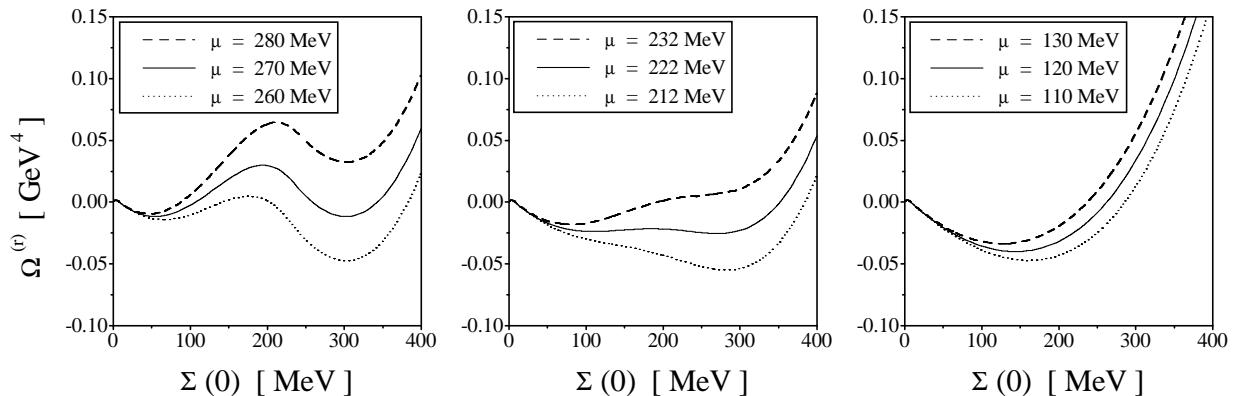


FIG. 4. Renormalized thermodynamic potential for Set II as a function of the selfenergy, for different values of the chemical potential μ . Left, central and right panels correspond to $T = 0$, $T = 50$ MeV and $T = 100$ MeV respectively.

The behaviour of the critical temperatures with the quark density is shown in Fig. 5, where we plot the $T-\rho$ phase diagrams for both the confining and the non-confining sets. The curves in the left panel correspond to the case of finite quark masses, and the fat dots indicate the end points for each set of parameters. The area below each curve is a region where both phases are allowed. This “mixed phase” zone can be interpreted [13] as a region where droplets containing light quarks of mass m_c coexist with a gas of constituent, massive quarks. The corresponding curves in the chiral case ($m_c = 0$) for both Sets I and II are shown in the right panel of the figure. Here the dotted lines correspond to the second order transitions, and the fat dots indicate the tricritical points.

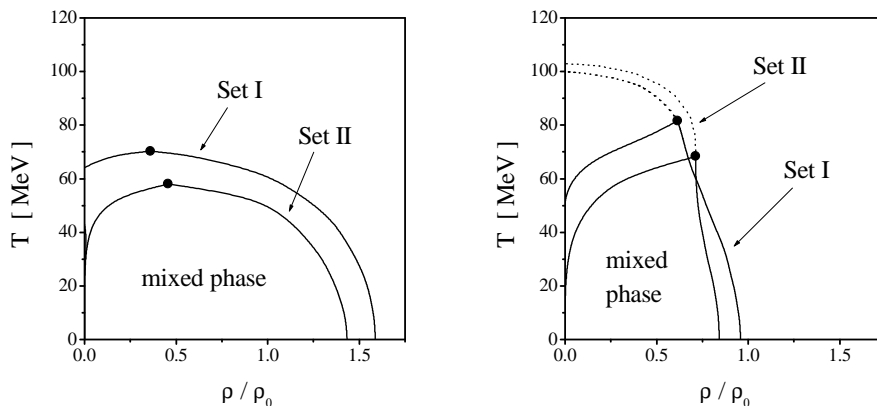


FIG. 5. Critical temperatures as functions of the relative density for Sets I and II. The left panel corresponds to the case of finite quark masses and the right panel to the chiral limit. The fat dots indicate the end points (left panel) and tricritical points (right panel), and the dotted lines in the right panel indicate the second order phase transitions.

It is interesting to discuss in detail the situation concerning the confining set. In this case we can find, for each temperature, the chemical potential μ_d at which confinement is lost. Following the proposal of Ref. [9], this corresponds to the point at which the selfenergy at zero momentum reaches the value $\Sigma(0)_{crit}$. Using the values of m_c and Λ corresponding to Set I we get $\Sigma(0)_{crit} = 267$ MeV. We see that for low temperatures the value of μ_d coincides with the chemical potential corresponding to the chiral restoration, while for temperatures close enough to that of the “end point” it starts to lie slightly below the phase

transition line. Above the end point temperature T_E it is difficult to make an accurate comparison since, for finite quark masses, the chiral restoration proceeds through a smooth crossover. However, we can still study the situation in the chiral limit. We find that in the region where the chiral phase transition is of second order deconfinement always occurs, for fixed T , at a lower value of μ than the chiral restoration. The corresponding critical line is indicated by a dashed line in the right panel of Fig. 3. In any case, as we can see in this figure, the departure of the line of chiral restoration from that of deconfinement is in general not too large. This indicates that within the present model both transitions tend to happen at, approximately, the same point.

B. Lorentzian regulator

Let us now consider the case of a Lorentzian regulator,

$$r(q^2) = \frac{1}{1 + (q^2/\Lambda^2)^n}, \quad (39)$$

where n is a positive integer. For this family of regulators, it can be seen that the quark propagator always has a finite number of poles in the q_0 plane. If n is even, there are $2n$ quartets of complex poles, plus a doublet of real poles. For odd values of n , one has a doublet (quartet) of real (complex) poles for $\bar{\Sigma}(0)$ below (above) a certain critical value $\bar{\Sigma}(0)_{crit}$, plus a set of $2n - 1$ quartets of complex poles, and a doublet of real poles. This last doublet occurs at $q_0^2 \gtrsim \Lambda^2$.

In order to analyze the characteristics of the chiral phase transition for this shape of the regulator, we have taken the simplest case $n = 1$, choosing as input parameter the quark selfenergy at zero temperature and chemical potential, $\bar{\Sigma}(0)$. As in the case of the Gaussian regulator, the parameters G , m_c and Λ have been fixed so as to reproduce correctly the physical values of the pion mass and decay constant. For a typical selfenergy $\bar{\Sigma}(0) = 300$ MeV we find the reasonable values $G = 28.38$ GeV $^{-2}$, $m_c = 4.57$ MeV and $\Lambda = 940$ MeV. The value of $\bar{\Sigma}(0)_{crit}$ is in this case approximately 270 MeV, hence the fermion propagator has two quartets and one doublet of poles. This is represented in Fig. 6.

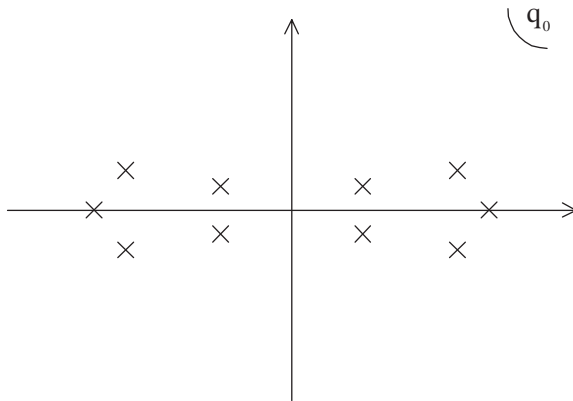


FIG. 6. Analytic structure of the quark propagator in the q_0 plane for an $n = 1$ Lorentzian regulator.

Once again, we can make use of both the gap equation and our result Eq.(34) to evaluate the quark self-energy $\Sigma(0)$ for given values of the temperature and chemical potential. The corresponding phase transition curves are plotted in the left panel of Fig. 7, where we have considered fixed temperatures of 0, 30, 50 and 100 MeV. As in the previous cases, we observe that for low values of T the chiral phase transition is of first order, while for values above a certain T_E the transition proceeds through a smooth crossover. In the right panel of the figure we plot for the same values of the temperature the relative quark density ρ/ρ_0 as a function of the chemical potential.

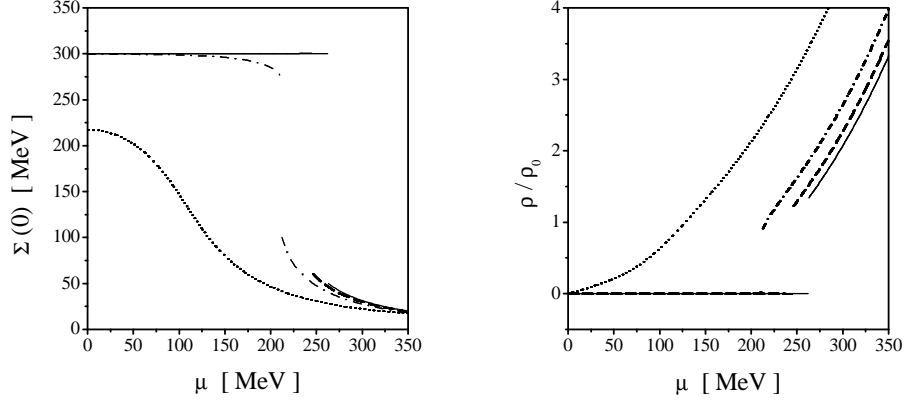


FIG. 7. Behaviour of the quark selfenergy (left) and the relative quark density (right) with the chemical potential in a non-local NJL model with a Lorentzian regulator, for some representative values of T . Full, dashed, dashed-dotted and dotted lines correspond to $T = 0, 30, 50$ and 100 MeV respectively.

It is interesting to point out that for temperatures quite below T_E (as e.g. 30 MeV for the present input parameters) and $\mu < \mu_c$ the selfenergy rises for increasing μ . Although the growth is too slight to be clearly perceived in the figure, it becomes evident at a magnified scale. Then, as T becomes closer to T_E , this behaviour turns into a decreasing one (see the $T = 50$ MeV curve in the left panel of Fig. 7), ending up in the smooth crossover at $T > T_E$. As mentioned in Sec. IV.a for the Gaussian interaction, the growing behaviour at low T is characteristic for the situation in which the Minkowski quark propagator has no real poles. We have stated above that for the Lorentzian regulator there is always a real pole close to $q_0^2 \gtrsim \Lambda^2$. Thus, we can argue that the rise of $\Sigma(0)$ is mainly related to the absence of real poles at low q_0^2 , which are in fact the poles to be associated with deconfined quarks. Moreover, this can be understood as a new evidence that the basic features of the $T - \mu$ behaviour of the quark properties are greatly determined by the first pole of the quark propagator.

The values of the critical temperature as a function of the chemical potential and the quark density are displayed in the left and right panels of Fig. 8, respectively. Once again, the $T - \rho$ phase diagram shows a mixed phase region. The predicted position of the end point is in this case $(T_E, \mu_E) = (58 \text{ MeV}, 195 \text{ MeV})$.

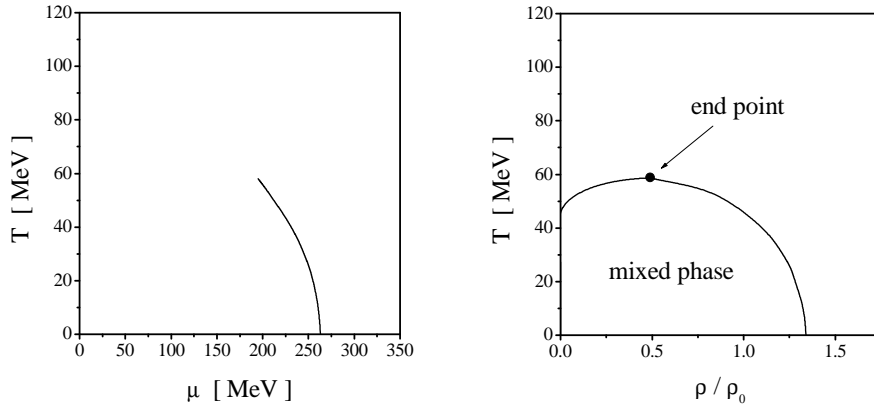


FIG. 8. Critical temperature for the Lorentzian regulator as a function of the chemical potential (left) and the relative quark density (right).

C. Instanton liquid model regulator

The instanton liquid picture of the QCD vacuum predicts a separable non-local interaction with a regulator given by

$$r(q^2) = -x \frac{d}{dx} [I_0(x)K_0(x) - I_1(x)K_1(x)] \Big|_{x=\sqrt{q^2}\rho/2}, \quad (40)$$

where I and K are the modified Bessel functions and ρ stands for the average instanton size. Here we take the standard value $\rho = 1/3$ fm, and fix the coupling constant to $G = 36.7$ GeV $^{-2}$ so as to reproduce the typical value for the instanton density $n \approx 1$ fm $^{-4}$ [5]. Using these values, together with $m_c = 4.9$ MeV, it is possible to reproduce the empirical values of the pion mass and decay constant. The resulting value of the chiral quark condensate at zero temperature and chemical potential is $-(256 \text{ MeV})^3$.

As in the previous cases, we can solve the gap equation to obtain the phase transition curve for the quark selfenergy $\Sigma(0)$. Here the situation is more complicated than for the Gaussian and Lorentzian cases, since the quark propagator has now a cut in the complex plane. As discussed in Sect. II, it is useful to look at the regulator function (40) in Minkowski space for zero three-momentum, $r(-q_0^2)$. If we consider the analytic extension in the complex q_0 plane, we see that the regulator shows a cut along the real axis, namely

$$r(-(x+i\epsilon)^2) - r(-(x-i\epsilon)^2) = 2i\pi [2\tilde{x}J_0(\tilde{x})J_1(\tilde{x}) - J_1(\tilde{x})^2], \quad (41)$$

with $\tilde{x} = \rho x/2$. It is easy to see that this cut is also present for the full quark propagator function. As stated in Sect. III, this translates into a cut on the real axis in the z plane if we set $q^2 = -(z+\mu)^2 + \vec{q}^2$. In addition, it can be seen that the quark propagator has a finite number of poles. The latter come in quartets, and their number increases with the value of the dimensionless parameter $\lambda \equiv \rho \bar{\Sigma}(0)$. One can find a set of critical values λ_i , such that there is only one quartet of complex poles for $0 < \lambda < \lambda_0$, two quartets for $\lambda_0 < \lambda < \lambda_1$, etc. The analytic structure of the propagator for the case of two quartets is illustrated in Fig. 9. The critical values λ_i only depend on the scaled current quark mass, ρm_c . Taking ρ and m_c as above we get for the first critical values $\lambda_0 \simeq 0.81$, $\lambda_1 \simeq 1.09$, $\lambda_2 \simeq 1.48$. With the chosen value $G = 36.7$ GeV $^{-2}$ the gap equation for $T = \mu = 0$ leads to $\bar{\Sigma}(0) = 359$ MeV, thus in our case $\lambda \simeq 0.6$ and we only have to consider a single quartet of complex poles. This means that the sum in Eq.(34) contains only one term.

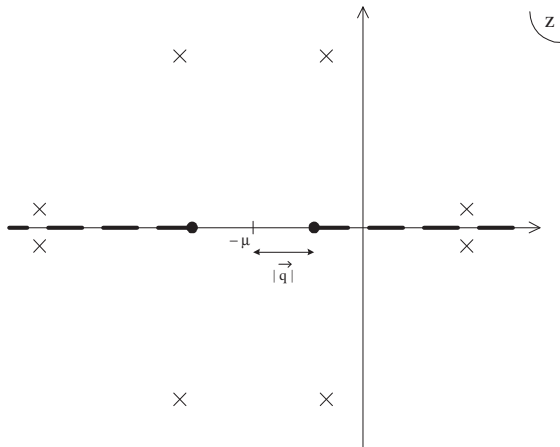


FIG. 9. Analytic structure of the quark propagator for the instanton liquid model.

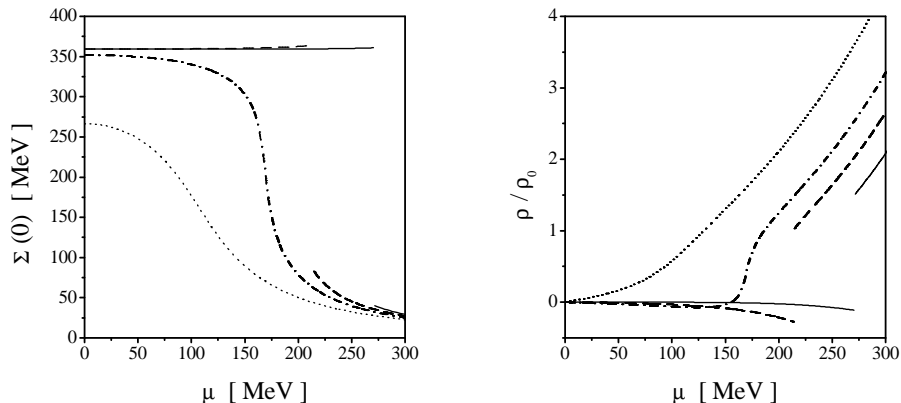


FIG. 10. Behaviour of the quark selfenergy (left) and the relative quark density (right) with the chemical potential for the instanton liquid model. Full, dashed, dashed-dotted and dotted lines correspond to $T = 0, 50, 70$ and 100 MeV respectively.

The behaviour of the quark selfenergy and the quark density as functions of the chemical potential are shown in Fig. 10 for some representative values of the temperature. Once again, we find that the transition is of first order for low values of T , turning into a smooth crossover above a certain end point. As in the confining Gaussian and Lorentzian cases, we find that for finite temperatures quite below T_E the selfenergy rises with μ for $\mu < \mu_c$. Thus, this feature does not seem to be dependent on the existence of the cut, though we have checked that its contribution to the corresponding gap equation is not negligible. Finally, as in the previous cases, we present the curves corresponding to the phase transition temperatures as functions of μ and ρ/ρ_0 . These are shown in Fig. 11. For the instanton liquid model the end point is found to be located at $(T_E, \mu_E) = (65 \text{ MeV}, 180 \text{ MeV})$.

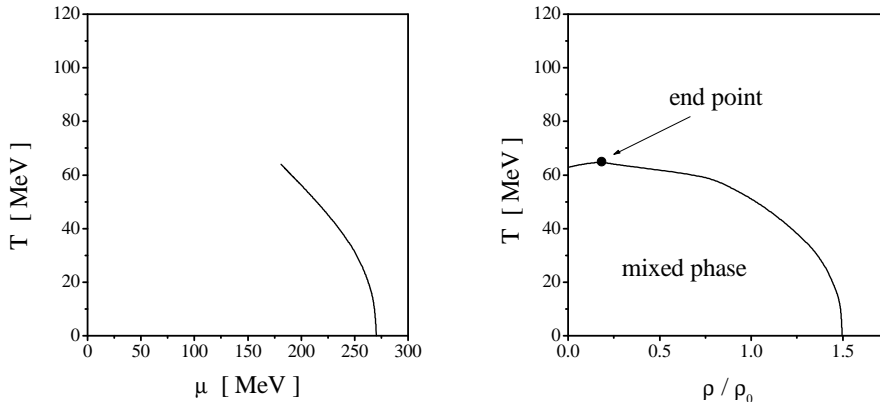


FIG. 11. Critical temperature for the instanton liquid model as a function of the chemical potential (left) and the relative quark density (right).

V. SUMMARY AND CONCLUSIONS

In this work we have studied the behaviour of chiral quark models with non-local covariant separable interactions at finite temperature and chemical potential. After introducing the general formalism we have derived some expressions that allow to compute the relevant quantities in terms of the analytic structure of the quark propagator. Although, in principle, the sum over the Matsubara frequencies could have been directly performed in a numerical way, we believe that our method allows for a better understanding of some features of the chiral restoration transition (as e.g. the importance of the first pole of the quark propagator) and stresses the connection with the usual procedure followed in the standard NJL model. In our numerical calculations we have considered three types of regulators: the Gaussian regulator, the Lorentzian regulator and the instanton liquid model regulator. In all these cases we have set the model parameters so as to reproduce the empirical values of the pion mass and decay constant and to get a chiral quark condensate in reasonable agreement to that determined from lattice gauge theory or QCD sum rules. We find that in all cases the phase diagram is quite similar. In particular, we obtain that for two light flavors the transition is of first order at low values of the temperature and becomes a smooth crossover at a certain “end point”. Our predictions for the position of this point are very similar for all the regulators and slightly smaller than the values in Refs. [13,14], $T_E \approx 100 \text{ MeV}$ and $\mu_E \approx 200 - 230 \text{ MeV}$. In this sense, we should remark that the model under consideration predicts a critical temperature at $\mu = 0$ of about 100 MeV [15], somewhat below the values obtained in modern lattice simulations which suggest $T_c \approx 140 - 190 \text{ MeV}$ [1]. In any case, our calculations seem to indicate that μ_E might be smaller than previously expected even in the absence of strangeness degrees of freedom.

An interesting feature of the behaviour of the quark selfenergy as a function of the chemical potential for temperatures well below T_E is that it raises with μ (for $\mu < \mu_c$) when the first pole in the quark propagator is complex. A similar behaviour is found for the chiral condensate [10]. This is the opposite to what happens when the first pole is real (in Minkowski space) as in the standard NJL model [3] or models where the nonlocality arises only in the space components [16]. Lattice calculations, even at very low chemical potential as e.g. those reported in Ref. [17], might be helpful to understand what happens in QCD.

Several extensions of this work are of great interest. For example, it would be very important to investigate the impact of the introduction of strangeness degrees of freedom and flavor mixing on the main features of

the chiral phase transition. In fact, some work on an $SU(3)$ extension of the present type of models at finite μ , but $T = 0$, has been recently reported [18]. Another topic that has recently attracted a lot of attention, and is suitable to be investigated in the present model, is the competition between chiral symmetry breaking and color superconductivity at large chemical potential. We expect to report on these issues in future publications.

ACKNOWLEDGMENTS

This work was supported in part by Fundación Antorchas and Fundación Balseiro, Argentina.

- [1] F. Karsch, *hep-lat/0106019*.
- [2] Y. Nambu and G. Jona-Lasinio, *Phys. Rev.* **122**, 345 (1961); *Phys. Rev.* **124**, 246 (1961).
- [3] U. Vogl and W. Weise, *Prog. Part. Nucl. Phys.* **27**, 195 (1991); S. Klevansky, *Rev. Mod. Phys.* **64**, 649 (1992); T. Hatsuda and T. Kunihiro, *Phys. Rep.* **247**, 221 (1994).
- [4] G. Ripka, *Quarks bound by chiral fields* (Oxford University Press, Oxford, 1997).
- [5] T. Schaefer and E. Shuryak, *Rev. Mod. Phys.* **70**, 323 (1998).
- [6] C.D. Roberts and A.G. Williams, *Prog. Part. Nucl. Phys.* **33**, 477 (1994); C.D. Roberts and S.M. Schmidt, *Prog. Part. Nucl. Phys.* **45S1**, 1 (2000).
- [7] E.R. Arriola and L.L. Salcedo, *Phys. Lett.* **B450**, 225 (1999).
- [8] G. Ripka, *Nucl. Phys.* **A683**, 463 (2001); R.S. Plant and M.C. Birse, *hep-ph/0007340*.
- [9] R.D. Bowler and M.C. Birse, *Nucl. Phys.* **A582**, 655 (1995); R.S. Plant and M.C. Birse, *Nucl. Phys.* **A628**, 607 (1998).
- [10] I. General, D. Gómez Dumm and N.N. Scoccola, *Phys. Lett. B* **506**, 267 (2001).
- [11] A.A. Abrikosov, Jr., *Nucl. Phys.* **B182**, 441 (1981); C.A. de Carvalho, *Nucl. Phys.* **B183**, 182 (1981).
- [12] G. W. Carter and D. Diakonov, *Phys. Rev. D* **60**, 016004 (1999).
- [13] J. Berges and K. Rajagopal, *Nucl.Phys.***B538**, 215 (1999).
- [14] M.A. Halasz *et al.*, *Phys.Rev.***D58**, 096007 (1998); M. Stephanov, K. Rajagopal and E. Shuryak, *Phys. Rev. Lett.* **81**, 4816 (1998); *Phys. Rev.* **D60**, 114028 (1999).
- [15] D. Blaschke, G. Burau, Y.L. Kalinovsky, P. Maris and P.C. Tandy, *Int. J. Mod. Phys. A* **16**, 2267 (2001); B. Szczerbińska and W. Broniowski, *Acta Phys. Polon.* **B31**, 835 (2000).
- [16] S.M. Schmidt, D. Blaschke and Y.L. Kalinovsky, *Phys. Rev. C* **50**, 435 (1994); D. Blaschke, Y.L. Kalinovsky, L. Munchow, V.N. Pervushin, G. Ropke and S.M. Schmidt, *Nucl. Phys. A* **586**, 711 (1995).
- [17] QCD-TARO Collaboration, *hep-ph/0107002*
- [18] C. Gocke, D. Blaschke, A. Khalatyan and H. Grigorian, *hep-ph/0104183*.